Experimental demonstration of wideband dispersion-compensated slow light by a chirped photonic crystal directional coupler

Daisuke Mori, Shousaku Kubo, Hirokazu Sasaki, and Toshihiko Baba

Yokohama National University, Department of Electrical and Computer Engineering
79-5 Tokiwadai, Hodogayaku, Yokohama 240-8501, Japan
Email: baba@ynu.ac.jp

Abstract: We report on the fabrication and evaluation of a directional coupler consisting of two different chirped photonic crystal (PC) waveguides that can generate wideband, low dispersion slow light. The directional coupler was fabricated from a silicon-on-insulator PC slab with airhole diameter chirping. For both waveguides, we observed a group index of 60–80 near the photonic band edge and opposite dispersion characteristics. In the directional coupler, we evaluated a group index of 30–40 in a wavelength bandwidth of 32 nm. The experimental results agree with the theoretical relation between the group index and bandwidth.

OCIS codes: (230.3990) Microstructure devices; (230.3120) Integrated Optics Device

References and links

1. T. Baba, N. Fukaya, and J. Yonekura, "Observation of light propagation in photonic crystal optical waveguides with bends," Electron. Lett. **35**, 654-655 (1999).
2. S. J. McNab, N. Moll, and Y. A. Vlasov, "Ultra-low loss photonic integrated circuit with membrane-type photonic crystal waveguides," Opt. Express **11**, 2927-2939 (2003).
3. Y. Sugimoto, Y. Tanaka, N. Ikeda, Y. Nakamura, K. Asakawa, and K. Inoue, "Low propagation loss of 0.76 dB/mm in GaAs-based single-line-defect two-dimensional photonic crystal slab waveguides up to 1 cm in length," Opt. Express **12**, 1090-1096 (2004).
4. E. Kuramochi, M. Notomi, S. Hughes, A. Shinya, T. Watanabe, and L. Ramunno, "Disorder-induced scattering loss of line-defect waveguides in photonic crystal slabs," Phys. Rev. B **72**, 161318 (2005).
5. M. Notomi, K. Yamada, A. Shinya, J. Takahashi, C. Takahashi, and I. Yokohama, "Extremely large group-velocity dispersion of line defect waveguides in photonic crystal slabs," Phys. Rev. Lett. **87**, 253902 (2001).
6. T. Asano, K. Kiyota, D. Kumamoto, B-S. Song, and S. Noda, "Time-domain measurement of picosecond light-pulse propagation in a two-dimensional photonic crystal-slab waveguide," Appl. Phys. Lett. **84**, 4690-4692 (2004).
7. M. Notomi, A. Shinya, S. Mitsugi, E. Kuramochi, and H. Ryu, "Waveguides, resonators and their coupled elements in photonic crystal slabs," Opt. Express **12**, 1551-1561 (2004).
8. Yu. A. Vlasov, M. O'Boyle, H. F. Hamann and S. J. McNab, "Active control of slow light on a chip with photonic crystal waveguides," Nature **438**, 65-69, (2005).
9. H. Gersen, T. J. Karle, R. J. P. Engelen, W. Bogaerts, J. P. Korterik, N. F. van Hulst, T. F. Krauss, and L. Kuipers, "Real-space observation of ultraslow light in photonic crystal waveguides," Phys. Rev. Lett. **94**, 073903 (2005).
10. K. Kiyota, T. Kise, N. Yokouchi, T. Ide, and T. Baba, "Various low group velocity effects in photonic crystal line defect waveguides and their demonstration by laser oscillation," Appl. Phys. Lett. **88**, 201904 (2006).
11. L. H. Frandsen, A. V. Lavrinenko, J. Fage-Pedersen, and P. I. Borel, "Photonic crystal waveguides with semi-slow light and tailored dispersion properties," Opt. Express **14**, 9444-9450 (2006).
12. M. F. Yanik, W. Suh, Z. Wang, and S. Fan, "Stopping light in a waveguide with an all-optical analog of electromagnetically induced transparency," Phys. Rev. Lett. **93**, 233903 (2004).
13. T. Baba, D. Mori, K. Inoshita, and Y. Kuroki, "Light localization in line defect photonic crystal waveguides," IEEE J. Sel. Top. Quantum Electron. **10**, 484-491 (2004).
14. D. Mori and T. Baba, "Dispersion-controlled optical group delay device by chirped photonic crystal waveguides," Appl. Phys. Lett. **85**, 1101-1103 (2004).

#79113 - $15.00 USD Received 17 Jan 2007; revised 11 Apr 2007; accepted 11 Apr 2007; published 16 Apr 2007

15. D. Mori and T. Baba, "Wideband and low dispersion slow light by chirped photonic crystal coupled waveguide," Opt. Express **13**, 9398-9408 (2005).
16. A. Sakai, G. Hara, and T. Baba, "Propagation characteristics of ultra-high Δ optical waveguide on silicon-on-insulator substrate," Jpn. J. Appl. Phys. **40**, L383-L385 (2001).
17. J. Zimmermann, B.K. Saravanan, R. März, M. Kamp, A. Forchel, and S. Anand, "Large dispersion in photonic crystal waveguide resonator," Electron Lett. **41**, 414-415 (2005).
18. S. Combrié, A. De Rossi, L. Morvan, S. Tonda, S. Cassette, D. Dolfi, and A. Talneau, "Time-delay measurement in singlemode, low-loss photonic crystal waveguides," Electron Lett. **42**, 86-88 (2006).

1. Introduction

Slow light having an ultralow group velocity v_g is of great interest because of its potential application to optical buffering and enhanced light-matter interaction. Photonic crystal (PC) waveguides [1–4] have been studied for use in generating slow light [5–11]. In general, slow light is constrained by the relation between the slowdown factor and operating spectral bandwidth. In addition, short optical pulses and high-bit-rate signals with a wide frequency spectrum are severely distorted due to large group velocity dispersion. Phase modulation of input signals by dynamic tuning of the material parameters has been discussed as a solution [12]. However, this method operates like a one-bit optical memory rather than an optical buffer because it cannot store continuous signals without mutual interference. Previously, we proposed and theoretically demonstrated a chirped PC waveguide whose structural parameters are gradually changed along the waveguide [13]. We also discussed combining the chirped structure with an ideal photonic band obtained by minute structural modifications to realize wideband, dispersion-compensated slow light [14,15]. In this case, the $v_g = 0$ condition obtained by a flat photonic band is set at an inflection point of the band. When such an ideal band is shifted in a chirped structure, a light pulse is first affected by the dispersion but is recovered by the opposite dispersion, and is delayed by the $v_g = 0$ condition. Such light propagation is obtained in a specified bandwidth by controlling the slope of the chirping. We showed theoretically that a directional coupler (DC) consisting of two different PC waveguides A and B with opposite dispersion characteristics equivalently realizes this operation [14].

In this paper, we experimentally demonstrate the operation of the DC. First, we briefly review the device structure and band profiles. Next, we explain the fabrication and evaluation methods. Then, we present the individual fabrication of A and B and evaluate the low v_g and opposite dispersion characteristics. Finally, we demonstrate wideband, dispersion-compensated slow light in the DC and discuss its correspondence with theoretical results.

2. Device and photonic band

The structures of the waveguides A and B and the DC are shown with their band profiles in Fig. 1. A PC slab, consisting of a triangular lattice of airholes in a Si slab, is used as a platform. Waveguide A in Fig. 1(a) is a simple line defect waveguide. Its transmission band in the photonic bandgap below the air light line shows dispersion from the band edge to higher frequencies. Waveguide B in Fig. 1(b) is a line defect waveguide in which small airholes are arranged at the center with a half-period offset. It has two transmission bands, though we focus on the lower frequency band showing dispersion to lower frequencies. The DC in Fig. 1(c) consists of waveguides A and B with an inter-waveguide spacing of three lines of airholes. It has three bands originating from A and B. The lower two bands with opposite dispersion characteristics are used for dispersion compensation. When these bands are shifted by a chirped structure and the band edge frequencies of these bands are maintained to be equal, directional coupling from A to B occurs within a very short length due to the $v_g = 0$ condition.

#79113 - $15.00 USD Received 17 Jan 2007; revised 11 Apr 2007; accepted 11 Apr 2007; published 16 Apr 2007

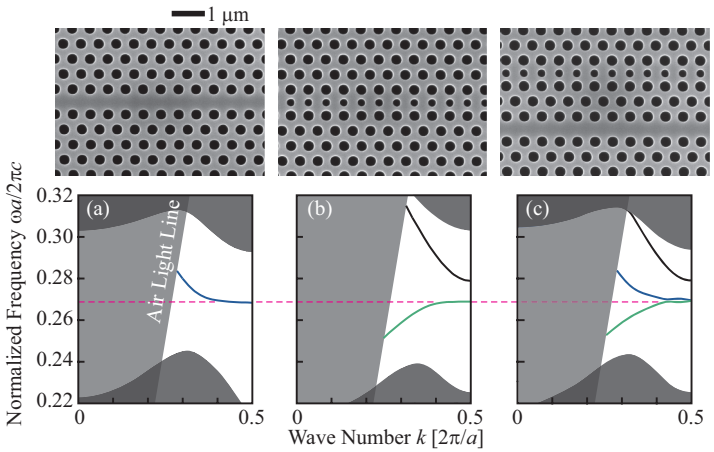

Fig. 1. Schematics of PC waveguide and corresponding bands calculated by plane wave expansion method. (a) A, (b) B, (c) DC. Blue and gray regions denote light cone and slab modes, respectively.

3. Experimental methods

The air-bridge PC slab was formed by *e*-beam lithography, SF_6 inductively coupled plasma etching and HF wet etching of the silicon-on-insulator substrate with a top Si layer of 0.213 μm thickness. First, A and B were fabricated and evaluated individually. The lattice constant a of A and B was set at 0.48 μm and the airhole diameters were set to $2r_1$ = 0.28 and 0.27 μm, respectively, so that the band edges were close to a wavelength of λ = 1.55 μm. For A, the line defect width defined by the distance between the centers of the innermost airholes was reduced to 85% of the simple line defect (*W*0.85) and the innermost airhole diameter of the waveguide was reduced by 5 nm. For B, *W*0.90 was used and the small airhole diameter $2r_2$ was 0.21 μm.

In the measurement, the group index $n_g = c/\upsilon_g$ was evaluated by two methods. In the first method (frequency-domain method), the inter-peak spacing $\Delta\lambda$ of the internal Fabry-Perot (FP) resonance is measured and n_g is obtained from the relation $n_g = \lambda^2/2L\Delta\lambda$, where L is the waveguide length [16,5]. It is a very simple method that requires measuring the transmission spectrum using a tunable laser source. The wavelength resolution of the laser source restricts the upper limit of the evaluated n_g and its accuracy is affected by disordering of the resonant spectrum. In the second method (modulation phase shift method), the shift of phase Φ between the input and output ends of the waveguide is measured for sinusoidally modulated light with frequency ω_m [7,8,11,17,18]. Although this method requires a more complicated setup, it allows direct evaluation of the delay time τ from the relation $\omega_m\tau = \Delta\Phi$. However, τ is increased or decreased when the internal FP resonance or antiresonance occurs, respectively. This effect can be eliminated and the n_g of the waveguide can be evaluated through the following analysis. The electric field E_o of the output light, which is a superposition of single pass and round-trip components of the FP resonance, is expressed as

$$E_o = E_i\sqrt{\left(1-r_i^2\right)\left(1-r_o^2\right)}\; e^{-\frac{1}{2}\alpha L - j\left(k_0 n_{eq}+\frac{\omega_m}{c}n_g\right)L} \Bigg/ \left[1 - r_i r_o e^{-\alpha L - j2\left(k_0 n_{eq}+\frac{\omega_m}{c}n_g\right)L - j(\phi_i+\phi_o)}\right] \qquad (1)$$

where E_i is the input electric field, r_i, r_o, ϕ_i, and ϕ_o are the amplitude and phase of the reflectivity at the input and output ends, respectively, α is the loss coefficient of the waveguide, $k_0 = 2\pi/\lambda$ and c are the wavenumber and velocity of light in vacuum, respectively, and n_{eq} is the equivalent index of the waveguide mode. In the absence of resonance, i.e. r_i, r_o =

#79113 - $15.00 USD Received 17 Jan 2007; revised 11 Apr 2007; accepted 11 Apr 2007; published 16 Apr 2007

0, the phase of E_o is given by that of the numerator of Eq. (1), i.e. $\Phi_n = -\omega_m n_g L/c$. When resonance occurs, the phase is modulated by the following phase of the denominator of Eq. (1):

$$\Phi_d \cong \tan^{-1}\left[\pm r_i r_o e^{-\alpha L} \sin\left(2\omega_m n_g L/c\right) \Big/ \left\{1 \mp r_i r_o e^{-\alpha L} \cos\left(2\omega_m n_g L/c\right)\right\}\right] \quad (2)$$

where the first plus and minus signs (and second minus and plus signs) correspond to the resonant and antiresonant conditions, respectively, which lead to over- and under-estimation of τ. The term $r_i r_o e^{-\alpha L}$ represents attenuation of light in the waveguide and can be evaluated from the amplitude of resonant fringes (peak to bottom ratio of the resonant transmission spectrum) [16]. Finally, n_g is determined such that the measured phase Φ equals $\Phi_n - \Phi_d$. Figure 2 shows the normalized phase shift $c\Delta\Phi/\omega_m L$ calculated with the amplitude of fringes. For each n_g assumed, larger and smaller phase shifts correspond to the resonance and antiresonance, respectively. In the absence of the resonance, the normalized phase shift becomes equivalent to n_g. When the amplitude of the fringes is larger than e.g. 5 dB, the phase shift oscillates in the range of twice. By fitting a theoretical curve with maximum and minimum phase shifts measured, n_g can be estimated.

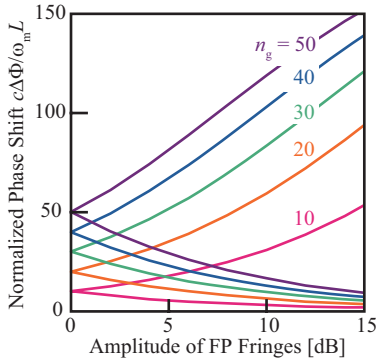

Fig. 2. Normalized phase shift calculated with amplitude of FP fringes. L = 120 μm and ω_m = 3 GHz were assumed. Upper line and lower line correspond to maximum and minimum phase shift caused by the resonance and antiresonance, respectively.

4. Results

Figure 3 shows measured transmission spectra and evaluated group index n_g. The light blue curve shows n_g obtained from the frequency-domain method. The red curve and circular data points show the normalized phase shift $c\Delta\Phi/\omega_m L$ and n_g obtained by the modulation phase shift method. Two methods give almost similar values of n_g. The band edge for A appears at the longer wavelength (lower frequency) side of the transmission band. As the wavelength approaches the band edge, n_g increases to 50. The band edge for B appears at the shorter wavelength (higher frequency) side. In this waveguide, FP resonance is particularly strong due to its higher facet reflectivity. Accordingly, the red curve oscillates widely between about 20 and 50. Nevertheless, the circular points are also in good agreement with the light blue frequency-domain curve and increase to 80. These results show that both A and B generate slow light near the band edge and they have opposite dispersion characteristics.

#79113 - $15.00 USD Received 17 Jan 2007; revised 11 Apr 2007; accepted 11 Apr 2007; published 16 Apr 2007

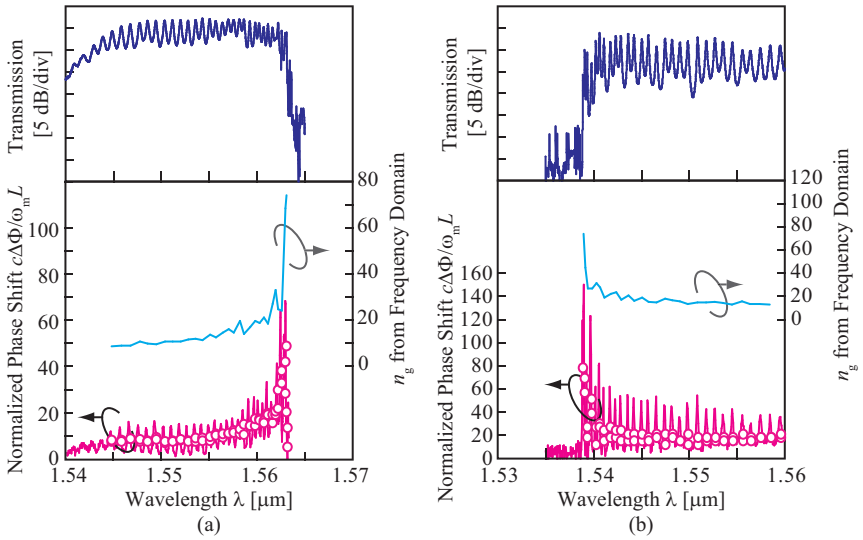

Fig. 3. Transmission spectra and n_g of (a) A and (b) B evaluated individually. In the n_g plots, the light blue curves were evaluated by frequency-domain method. The red curves and circular data points indicate normalized phase shift and evaluated n_g, respectively, by modulation phase shift method.

For the DC, the parameters were set to a = 0.48 μm and $2r_2$ = 0.21 μm. For simple fabrication, chirping was introduced into $2r_1$ by controlling the *e*-beam exposure time. In the chirping, a linear change of $2r_1$ from 0.27 to 0.29 μm was obtained over a device length L of 120 μm with a local fluctuation of ±5 nm. In the device, the precise matching of two band-edges is crucial for high efficiency light transmission. We reduced the difference between the band-edge wavelengths of A and B to less than 5 nm by fine tuning the line defect width of A around *W*0.85 and the innermost airhole diameter. In the measurement, light was incident on A. When the wavelength was too short, the light was directly output from A even in the chirped structure. When the wavelength was in the target range, light reached the band-edge position and was output from B through the directional coupling. Figure 4 shows transmission spectra observed at the output ends of A and B. The light output was switched from A to B at λ = 1.525 μm and directional coupling occurred for a wavelength bandwidth of 32 nm at longer wavelengths. The maximum output intensity from B was 3 dB lower than that from A, and the spectrum for B exhibits large fringes of 5–15 dB. These might be caused by a small mismatch of the band edges and insufficient smoothness of the chirping, which lead to nonuniform reflection and localization of light at the directional coupling points. The fringes, which look to be arising from simple FP resonances, have amplitudes of 5–10 dB. Therefore, larger amplitudes of some spectral dips might be caused by the above imperfections. To investigate this effect, we calculated the transmission spectrum in the device using finite-difference time-domain (FDTD) method. Due to the limitation of computer resources, we did not directly model the device with a fluctuation in airhole diameter of a few nanometers, but assumed a small and random fluctuation in slab index, which corresponds to the airhole diameter fluctuation. In this calculation, we found that the spectral fringes can be almost eliminated if the airhole diameter fluctuation is reduced to ±2 nm (<1% of the airhole diameter). The solid curve in Fig. 5 shows the normalized phase shift $c\Delta\Phi/\omega_m L$ measured by the modulation phase shift method. Similarly to the case of Fig. 3, it oscillates according to the spectral fringes. However, the minimum line is larger than 25. This means that the average group index $\tilde{n}_g$ in the chirped structure is larger than this value over the transmission bandwidth. We evaluated $\tilde{n}_g$ for some FP-like fringes using the experimental data analysis

#79113 - $15.00 USD Received 17 Jan 2007; revised 11 Apr 2007; accepted 11 Apr 2007; published 16 Apr 2007

explained in Section 3. As shown by the circular data points in Fig. 5, $\tilde{n}_g$ lies in the range of 30–40.

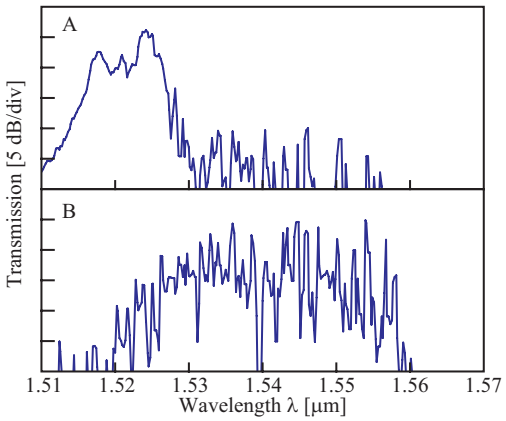

Fig. 4. Transmission spectra of chirped directional coupler obtained from the output ends of A and B (top and bottom plots, respectively).

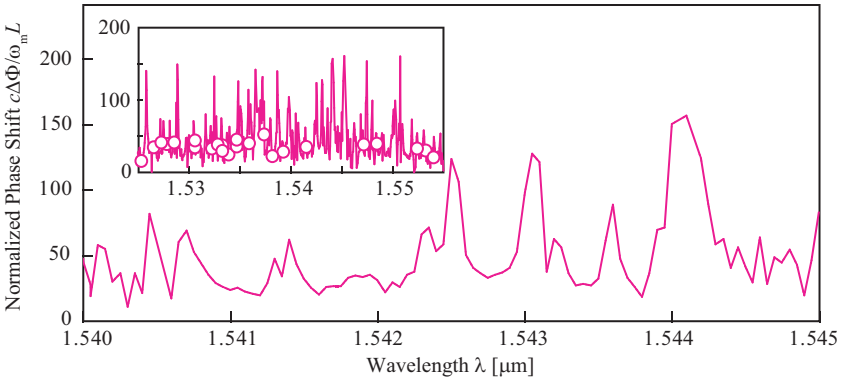

Fig. 5. Result of modulation phase shift measurement for chirped DC. Red curves and circular data points indicate normalized phase shift and evaluated $\tilde{n}_g$, respectively.

5. Comparison with calculation results

As discussed in Ref. [15], $\tilde{n}_g$ is constrained by the bandwidth even in chirped structures. The balance between $\tilde{n}_g$ and the bandwidth is changed by the slope and range of the chirping (change of structural parameters between the start and end points of the chirping against the chirped length); a smaller slope gives a larger $\tilde{n}_g$ and a narrower bandwidth. This relationship was confirmed by a summary of $\tilde{n}_g$ for sample devices shown in Fig. 6. The circles and error-bars indicate the average and fluctuation of $\tilde{n}_g$ over the bandwidth, respectively. The solid line shows a theoretical value obtained by band calculations. The experimental plots for Fig. 5 agree well with the theoretical value. Here, the theoretical value saturates to nearly 100 at the narrow bandwidth limit. This saturation is caused by distortion of coupled bands near the band edge, as shown in Fig. 1(c), which reduces the useful bandwidth. The band distortion can be eliminated by expanding the inter-waveguide spacing of A and B and reducing the coupling strength. Under these conditions, an ideal increase in $\tilde{n}_g$, as shown by the dashed

#79113 - $15.00 USD Received 17 Jan 2007; revised 11 Apr 2007; accepted 11 Apr 2007; published 16 Apr 2007

line in Fig. 6, is expected; i.e. $\tilde{n}_g$ = 550 for a normalized bandwidth $\Delta\omega/\omega = 2.06\times10^{-4}$ (40 GHz at λ = 1.55 μm).

It should be noted, however, that there is a limit to the increase in $\tilde{n}_g$ actually because the narrow bandwidth operation is disturbed by the fluctuation in airhole diameter. For example, the fluctuation of ±5 nm in our fabrication corresponds to half of the total chirping range of $2r_1$ = 0.27 – 0.29 μm and the operating bandwidth is 32 nm ($\Delta\omega/\omega = 2.06\times10^{-2}$). This means that half of this bandwidth, i.e. 16 nm is the limit to be realized. In fact, device samples with narrower chirping ranges were fabricated and the narrowing of the operating bandwidth was observed up to this value. However, the increase in $\tilde{n}_g$ was almost saturated, as shown by experimental plots in Fig. 6. The fluctuation can be reduced to ±0.5 nm by improving the *e*-beam lithography; ±1 nm was achieved by the present technology [4], and further improvement is expected in future. Then, $\tilde{n}_g$ = 200 for the bandwidth of 3 nm ($\Delta\omega/\omega = 2.06\times10^{-3}$) will be available.

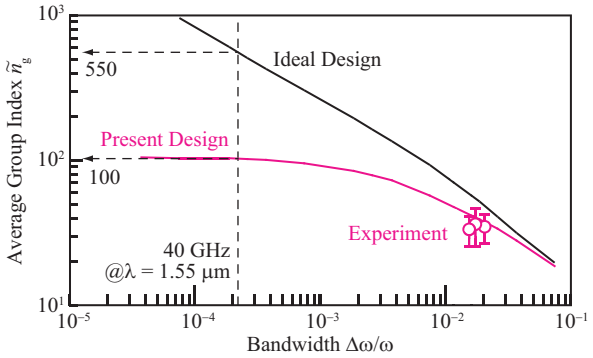

Fig. 6. Experimental and theoretical values of $\tilde{n}_g$.

6. Conclusion

In this paper, we fabricated two kinds of PC waveguides with opposite dispersion characteristics, and demonstrated wideband, dispersion-compensated slow light in a chirped PC directional coupler consisting of these waveguides. In the device, the average group index $\tilde{n}_g$ was 30–40 in a wide wavelength bandwidth of 32 nm. The relation between $\tilde{n}_g$ and bandwidth agrees with the theoretical calculation. Structural optimizations can enhance $\tilde{n}_g$ to, at least, 200 by narrowing the operating bandwidth to 3 nm at λ = 1.55 μm. Completely flat transmission and group index spectra are crucial for more precise evaluation of the group index, narrowing the bandwidth, and practical use of this device. For this purpose, more precise matching of band edges, smoothing of the chirping, and the use of anti-reflection structure at the input and output facets are important future issues.

Acknowledgments

This work was partly supported by The CREST Project of JST, The IT program and The 21st Century COE program of MEXT, and The Grant-In-Aid and The Research Fellowship of JSPS.

#79113 - $15.00 USD Received 17 Jan 2007; revised 11 Apr 2007; accepted 11 Apr 2007; published 16 Apr 2007